P8.9 Supercell Dissipation Observed by VORTEX2 on 9 June 2009

Casey E. Letkewicz* and Matthew D. Parker
North Carolina State University, Raleigh, North Carolina

1. INTRODUCTION

Understanding the dynamics of supercell thunderstorms has been a long-standing area of active research, often with a focus on the developing and mature stages of the storm (e.g., Browning 1964, Klemp et al. 1981, Davies-Jones 1984, Brandes 1988, Droegemeier et al. 1993, Weisman and Rotunno 2000, Davies-Jones 2002; see a summary in Bluestein 2007). More recently, supercell research has expanded to explore the processes behind weakening and dissipating supercells (Bluestein 2008, Ziegler et al. 2010). Supercell decay has often been attributed to movement into cooler, more stable air (Bluestein 2008), though storms that move along a baroclinic boundary also appear to be much more likely to be long-lived (Bunkers et al. 2006) and produce a tornado (Maddox et al. 1980, Markowski et al. 1998a). While many past supercell studies have investigated the dynamics via idealized simulations with homogeneous base-state conditions, environmental heterogeneities can have a significant impact on storm evolution (Markowski et al. 1998b, Atkins et al. 1999, Kost 2004, Richardson et al. 2007). Anticipating storm evolution is vital for operational forecasters, particularly as it concerns the issuance and duration of severe warnings, in turn affecting the false alarm rate. Additionally, future convective activity can be impacted by remnant convective boundaries; thus, an improved understanding of the processes behind supercell dissipation would aid in short-term forecasts of convection.

On 9 June 2009, the Verification of the Origins of Rotation in Tornadoes Experiment 2 (VORTEX2) sampled a supercell in southcentral Kansas that produced strong low-level rotation and generated at least one reported tornado. However, an hour after the VORTEX2 armada deployed its various assets, the storm updraft was observed to shrink and completely dissipate. Mindful of the influence of mesoscale heteorogeneities and taking advantage of the many VORTEX2 assets sampling this storm, the goal of this study is to understand the mechanisms leading to the decay of this supercell.

*Corresponding author address: Casey E. Letkewicz, Department of Marine, Earth, & Atmospheric Sciences, North Carolina State University, Campus Box 8208, Raleigh, NC 27695–8208. E-mail: celetkew@ncsu.edu

Section 2 will detail the evolution of the storm and its environment just prior to and during dissipation; Section 3 will speculate on the chain of events and processes leading to decay, and Section 4 will present conclusions and future work.

2. STORM EVOLUTION

a. *Data and Methodology*

Coordinated sampling of this supercell and its mesoscale environment was achieved with numerous VORTEX2 instrument platforms. In the present study, data from select platforms will be utilized to demonstrate the storm-scale morphology. The supercell's inflow environment will be described by soundings launched by the NSSL1 vehicle using the mobile GPS advanced upper air sounding system (MGAUS), while the evolution of the storm itself will be illustrated by radar data from the two Shared Mobile Atmospheric Research and Teaching radars (SMART-Rs; Biggerstaff et al. 2005).

Dual-Doppler coverage was available from the SMART-Rs just prior to and during storm dissipation, approximately 2345-0021 UTC. The data was interpolated onto a $60 \times 60 \times 15$ km Cartesian grid using a two-pass Barnes analysis scheme (Barnes 1964), with a horizontal and vertical grid spacing of 500 m. A flat lower boundary was used, with the bottom of the grid defined to be the mean elevation of the two radars. A correction for storm motion (9.8 ms^{-1} from 290°) was included to account for the time required to complete a volume scan (approximately 3 minutes). The three-dimensional wind syntheses were constructed using upward integration of mass continuity with a lower boundary condition of $w = 0$. For brevity, only select volume scans will be presented.

b. *Local Environment*

Three inflow soundings were launched throughout the lifetime of the supercell, at 2319, 2354, and 0056 UTC. Vertical profiles of convective available potential energy (CAPE) and convective inhibition (CIN) in Fig. 1 illustrate the modifications to the thermodynamic environment over time. Instability notably *increased* from

2319 to 2354 UTC, associated with low-level moistening (not shown). CIN generally increased over time, though not strongly so until 0056 UTC (after storm dissipation), thus it is unclear whether the increases in CIN alone resulted in storm demise. Nowotarski and Markowski (2008) have shown that the addition of a shallow stable layer does not alter the strength of an idealized supercell's updraft or mid-level rotation, though it does weaken low-level updrafts and vertical vorticity. In the present case, strong low-level rotation and a possible funnel were reported around 2354 UTC, demonstrating that the increase in CIN from 2319 to 2354 UTC did not appear to significantly influence the supercell. However, it is likely that the strong increase in CIN after 2354 UTC did contribute to storm demise by suppressing low-level updrafts as the storm decayed.

The inflow wind profile also exhibited substantial changes over the lifetime of the storm. Fig. 2 illustrates these changes in the wind profile, with winds near the surface backing over time, acquiring a hairpin shape, and a straightening of the hodograph in the mid-levels. The hairpin in the low-levels indicates the passage of a boundary, which acted to modify both the instability (as discussed above) and the wind profile. Shear and helicity parameters reflect these modifications, with slight increases in 0-1 and 0-3 km bulk shear, decreases in 0-6 km bulk shear and effective shear, and a strong decrease in 0-3 km and effective storm-relative helicity (Table 1; effective parameters were defined as in Thompson et al. 2003). These changes in shear and SRH could impact storm maintenance in a few ways: 1) changes to the rate at which horizontal streamwise vorticity is fluxed into the supercell and tilted into updraft helicity; 2) changes to the dynamical lifting associated with the "updraft in shear" effect (i.e., linear forcing described in Rotunno and Klemp 1982); 3) cold pool-shear interactions that affect lifting along the supercell's cold pool. To elucidate the extent to which any of these hypothesized effects influenced the storm's evolution, analysis of the dual-Doppler-derived 3D wind field will be utilized, and is discussed next.

c. *Dual-Doppler Analysis*

At the beginning of the dual-Doppler synthesis at 2345 UTC, there was a clear sense of low- and mid-level updraft rotation (Fig. 3). However, this strong rotation was quickly lost within the next few volume scans, and had not redeveloped by the end of the SMART-R dual-Doppler deployment at 0021 UTC (Figs. 4-6). During this same period, updraft velocities generally weakened, though some restrengthening was evident in the last available volume scan (Fig. 7). Given the ample CAPE and small modifications in CIN before this period, these changes to the strength of the updraft appear to have been the result of the observed modification in low- and mid-level rotation. Examination of updraft helicity (calculated in the manner of Kain et al. 2008) values reveal a steep decline during the analysis period (Fig. 8), coincident with the sharp decrease in effective SRH (Table 1). The resurgence in updraft helicity at 0021 UTC was a result of the stronger updraft, rather than an increase in vertical vorticity (not shown). The general decline in updraft rotation points to the influence of the weakening SRH, whereby the flux of horizontal streamwise vorticity into the storm continually decreased, leading to weaker updraft rotation. With weaker updraft rotation, dynamic lifting via the nonlinear "spin" effect (Weisman and Rotunno 2000) would also weaken, resulting in a gradual decline in vertical velocities.

As the updraft continued to weaken, hydrometeors began to fall out in the rear flank. This precipitation appeared to be "left behind" as the storm continued to move downstream, evident on the western edge of the storm at the surface by 0003 UTC (shown here at 0009 UTC in Fig. 5). Coincident with this precipitation fallout was an increasingly divergent rear flank outflow. The outflow initially surged at 2357 UTC (Fig. 4), but as the divergence increased, surface winds behind the rear flank gust front began to back, becoming northeasterly by 0009 UTC (Fig. 5). These changes in the rear flank resulted in a gust front reorientation (Fig. 9), where it became more parallel to the low-level shear vector (Fig. 2). This in turn weakened low-level lifting, evident by the decline in low-level velocities in Fig. 7. Additionally, photos of the storm starting around 0000 UTC document a downstream tilt of the updraft, indicating a non-optimal "balance" between the cold pool and low-level shear (Rotunno et al. 1988). The cold pool temperature deficit remained around 3-4 K prior to and during the outflow reorientation (based on Sticknet and mobile mesonet data; not shown), suggesting that the modified updraft tilt could be explained by the changing gust front-perpendicular shear. However, the cold pool depth is unknown (not sampled), and whether the gust front-perpendicular shear changes would actually result in the observed updraft tilt is still unclear. Data from shorter-wavelength radars may help to elucidate the cold pool structure, low-level lifting, and evolving gust front updraft tilt.

Despite the overall decline in vertical velocity, a resurgence in updraft strength occurred toward the end of the dual-Doppler deployment (Fig. 7). Given the decrease in SRH and potential contributions of the changing low-level shear, we speculate that the storm evolved towards a multicell-type storm, with pulses in updraft strength governed by lifting along the gust front. However, additional dual-Doppler analyses after 0021 UTC

(unavailable from the SMART-Rs) are necessary to verify this claim.

3. PROCESSES LEADING TO DECAY

The dissipation of the supercell on 9 June 2009 was the result of the storm moving into a changing thermodynamic and kinematic environment. We speculate that the trends in shear and helicity primarily led to storm decay through a series of processes working concurrently, while the increasing CIN contributed to dissipation, particularly towards the end of the storm's life. Based on our assessment of the dual-Doppler data, we hypothesize that the following chain of events lead to storm demise. As the supercell moved into an environment with smaller effective SRH, the smaller flux of horizontal streamwise vorticity resulted in weaker updraft rotation. In turn, this had two effects: 1) an increasingly multicellular structure; and 2) a weakening of dynamic lifting and vertical velocities via nonlinear effects. As the updraft weakened, precipitation fell out into the rear flank, initially creating a surge in the outflow, later resulting in broad divergence in the rear flank. These modifications to the outflow produced a reorientation of the rear flank gust front, where it became more parallel to the low-level shear vector, which would be expected to weaken the low-level lifting. We also speculate that this combination of processes caused the supercell to transition towards an increasingly weak multicell regime, with a few pulses in the updraft as the storm decayed. The trends in shear and helicity, as well as CIN, reinforced the process, eventually resulting in complete storm dissipation.

While there is evidence that the decline in effective SRH and the changing low-level shear influenced the evolution of the supercell, it is less clear the extent to which the "updraft in shear" effect impacted the dynamic lifting and storm decay. The 0-6 km and effective bulk shear magnitudes showed minor changes between 2319 and 2354 UTC, but later exhibited weakening. We hypothesize that this effect may have contributed to storm dissipation later on by weakening the dynamic lifting, but did not instigate the decay process.

4. CONCLUSIONS AND FUTURE WORK

The changing inflow environment on 9 June 2009 appears to have lead to the dissipation of the supercell targeted by VORTEX2. We conclude that the changing shear and helicity lead to a series of events resulting in storm demise, with contributions by the increasing low-level stability. As the storm encountered weaker effective SRH, updraft rotation decreased, consequently weakening the vertical velocities. The precipitation core then fell out into the rear flank, producing increasingly divergent outflow and reorienting the gust front more parallel to the low-level shear vector. In turn, the low-level lifting weakened, aided by the increasing CIN, further contributing to the decline in storm strength.

Several questions remain regarding the evolution of this storm. For example, what were the updraft characteristics prior to 2345 UTC? Was the supercell already in a state of decline at the beginning of the dual-Doppler deployment? Did the updraft continue to "pulse" after 0021 UTC, consistent with an evolution towards a multicell? Additional radar data will need to be examined to pursue these avenues and establish a complete timeline of storm growth and decay. Characterization of the low-level lifting and rear flank outflow in relation to the changes in the updraft throughout the storm's lifetime will elucidate the contribution cold pool-shear interactions and clarify the chain of events and processes leading to demise. Numerical simulations incorporating the observed changes in the inflow environment could test the extent to which each of the three hypothesized influences of the wind profile either instigated or contributed to supercell dissipation, as well as the role of the increasing low-level stability. Finally, analysis of additional cases from VORTEX2 would help assess the generality of the processes leading to supercell demise. Pursuit of these avenues will promote greater understanding of the circumstances resulting in storm dissipation.

Acknowledgments. The authors would like to acknowledge Conrad Ziegler and Mike Biggerstaff for providing the edited SMART-R data used for the dual-Doppler analysis. David Dowell provided the code to perform the radar objective analysis and dual-Doppler synthesis, with modifications by Paul Markowski. Thanks also go to the Convective Storms Group at NC State University for their assistance and feedback. The research reported here is supported by the National Science Foundation under Grant ATM-0758509.

References

Atkins, N. T., M. L. Weisman, and L. J. Wicker, 1999: The influence of preexisting boundaries on supercell evolution. *Mon. Wea. Rev.*, **127**, 2910–2927.

Barnes, S. L., 1964: A technique for maximizing details in numerical weather map analysis. *J. Appl. Meteor.*, **3**, 396–409.

Biggerstaff, M. I., L. J. Wicker, J. Guynes, C. Ziegler, J. M. Straka, E. N. Rasmussen, A. Doggett, IV, L. D. Carey, J. L. Schroeder, and C. Weiss, 2005: The shared mobile atmospheric research and teaching radar. *Bull. Amer. Meteor. Soc.*, **86**, 1263–1274.

Bluestein, H. B., 2007: Advances in applications of the physics of fluids to severe weather systems. *Rep. Prog. Phys.*, **70**, 1259–1323.

Bluestein, H. B., 2008: On the decay of supercells through a "downscale transition": Visual documentation. *Mon. Wea. Rev.*, **136**, 4013–4028.

Brandes, E. A., 1988: Streamwise vorticity effects on supercell morphology and persistence. *J. Atmos. Sci.*, **45**, 947–963.

Browning, K. A., 1964: Airflow and precipitation trajectories within severe local storms which travel to the right of the mean wind. *J. Atmos. Sci.*, **21**, 634–639.

Bunkers, M. J., M. R. Hjelmfelt, and P. L. Smith, 2006: An observational examination of long-lived supercells. Part I: Characteristics, evolution, and demise. *Wea. Forecasting*, **21**, 673–688.

Davies-Jones, R., 1984: Streamwise vorticity: The origin of updraft rotation in supercell storms. *J. Atmos. Sci.*, **41**, 2991–3006.

Davies-Jones, R., 2002: Linear and nonlinear propagation of supercell storms. *J. Atmos. Sci.*, **59**, 3178–3205.

Droegemeier, K. K., S. M. Lazarus, and R. Davies-Jones, 1993: The influence of helicity on numerically simulated convective storms. *Mon. Wea. Rev.*, **121**, 2005–2029.

Kain, J. S., S. J. Weiss, D. R. Bright, M. E. Baldwin, J. J. Levit, G. W. Carbin, C. S. Schwartz, M. L. Weisman, K. K. Droegemeier, D. B. Weber, and K. W. Thomas, 2008: Some practical considerations regarding horizontal resolution in the first generation of operational convection-allowing NWP. *Wea. Forecasting*, **23**, 931–952.

Klemp, J. B., R. B. Wilhelmson, and P. S. Ray, 1981: Observed and numerically simulated structure of a mature supercell thunderstorm. *J. Atmos. Sci.*, **38**, 1558–1580.

Kost, J. K., 2004: Impacts of temporally variable environmental vertical wind shear upon numerically simulated convective storms. M.S. thesis, The Pennsylvania State University.

Maddox, R. A., R. Hoxit, and C. F. Chappell, 1980: A study of tornadic thunderstorm interactions with thermal boundaries. *Mon. Wea. Rev.*, **108**, 322–336.

Markowski, P. M., E. N. Rasmussen, and J. M. Straka, 1998a: The occurrence of tornadoes in supercells interacting with boundaries during VORTEX-95. *Wea. Forecasting*, **13**, 852–859.

Markowski, P. M., J. M. Straka, E. N. Rasmussen, and D. O. Blanchard, 1998b: Variability of storm-relative helicity during VORTEX. *Mon. Wea. Rev.*, **126**, 2959–2971.

Nowotarski, C. J., and P. M. Markowski, 2008: The effects of varying low-level, environmental stability on low-level rotation in numerical simulations of elevated supercells. Preprints, *24th Conf. Severe Local Storms*, Savannah, GA, Amer. Meteor. Soc.

Richardson, Y. P., K. K. Droegemeier, and R. P. Davies-Jones, 2007: The influence of horizontal environmental variability on numerically simulated convective storms. Part I: Variations in vertical shear. *Mon. Wea. Rev.*, **135**, 3429–3455.

Rotunno, R., and J. B. Klemp, 1982: The influence of the shear–induced pressure gradient on thunderstorm motion. *Mon. Wea. Rev.*, **110**, 136–151.

Rotunno, R., J. B. Klemp, and M. L. Weisman, 1988: A theory for strong, long–lived squall lines. *J. Atmos. Sci.*, **45**, 463–485.

Thompson, R. L., R. Edwards, J. A. Hart, K. L. Elmore, and P. Markowski, 2003: Close proximity soundings within supercell environments obtained from the Rapid Update Cycle. *Wea. Forecasting*, **18**, 1243–1261.

Weisman, M. L., and R. Rotunno, 2000: The use of vertical wind shear versus helicity in interpreting supercell dynamics. *J. Atmos. Sci.*, **57**, 1452–1472.

Ziegler, C. L., E. R. Mansell, J. M. Straka, D. R. MacGorman, and D. W. Burgess, 2010: The impact of spatial variations of low-level stability on the lifecycle of a simulated supercell storm. *Mon. Wea. Rev.*, **138**, 1738–1766.

	2319 UTC	**2354 UTC**	**0056 UTC**
0-6 km shear (ms^{-1})	31.9	29.0	24.4
0-3 km shear (ms^{-1})	14.8	17.0	20.0
0-1 km shear (ms^{-1})	1.8	5.7	5.9
Effective shear (ms^{-1})	18.7	19.5	11.3
0-3 km SRH (m^2s^{-2})	232	183	68
Effective SRH (m^2s^{-2})	180	127	47

Table 1: Shear and storm-relative helicity (SRH) parameters computed from the NSSL1 inflow soundings. Effective parameters were defined as in Thompson et al. (2003).

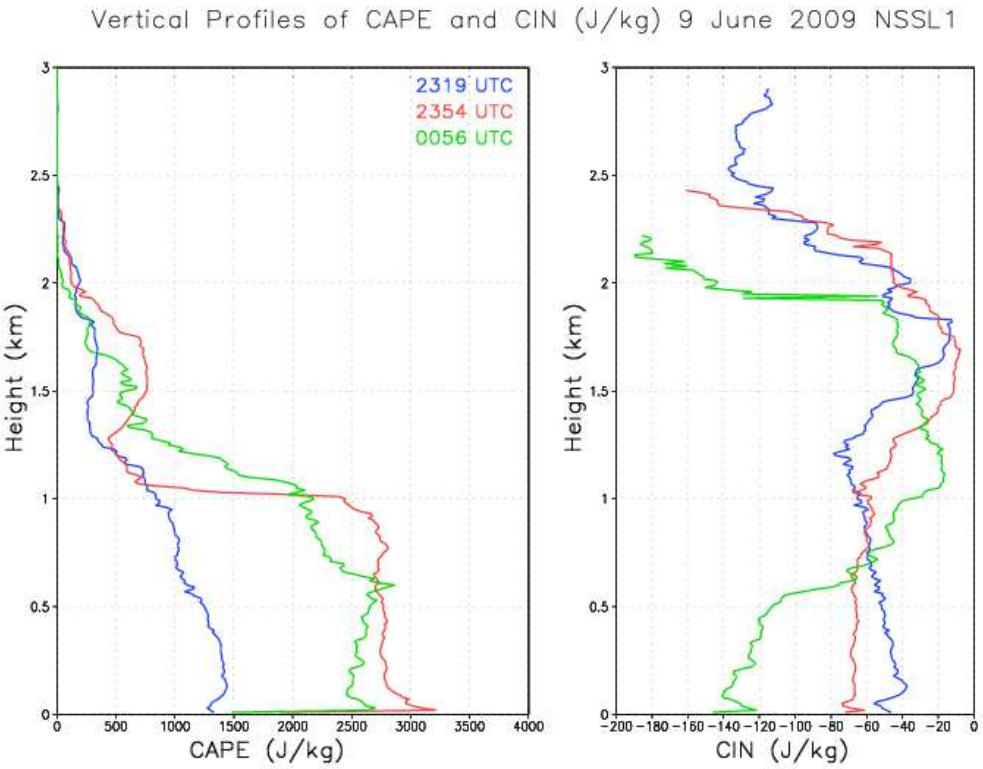

Figure 1: Vertical profiles of CAPE and CIN (Jkg^{-1})from the NSSL1 inflow soundings over time.

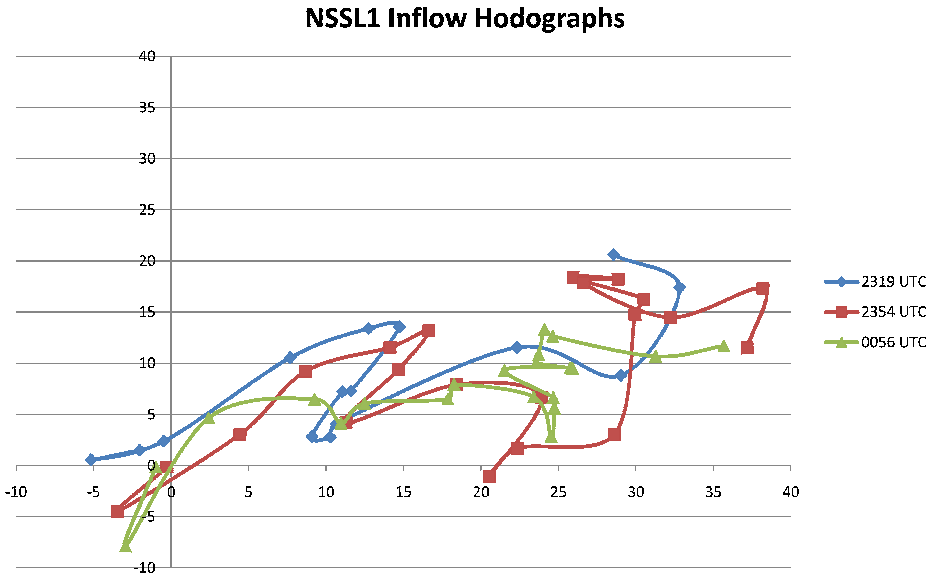

Figure 2: Hodographs from the NSSL1 inflow soundings over time, with markers placed every 500 m.

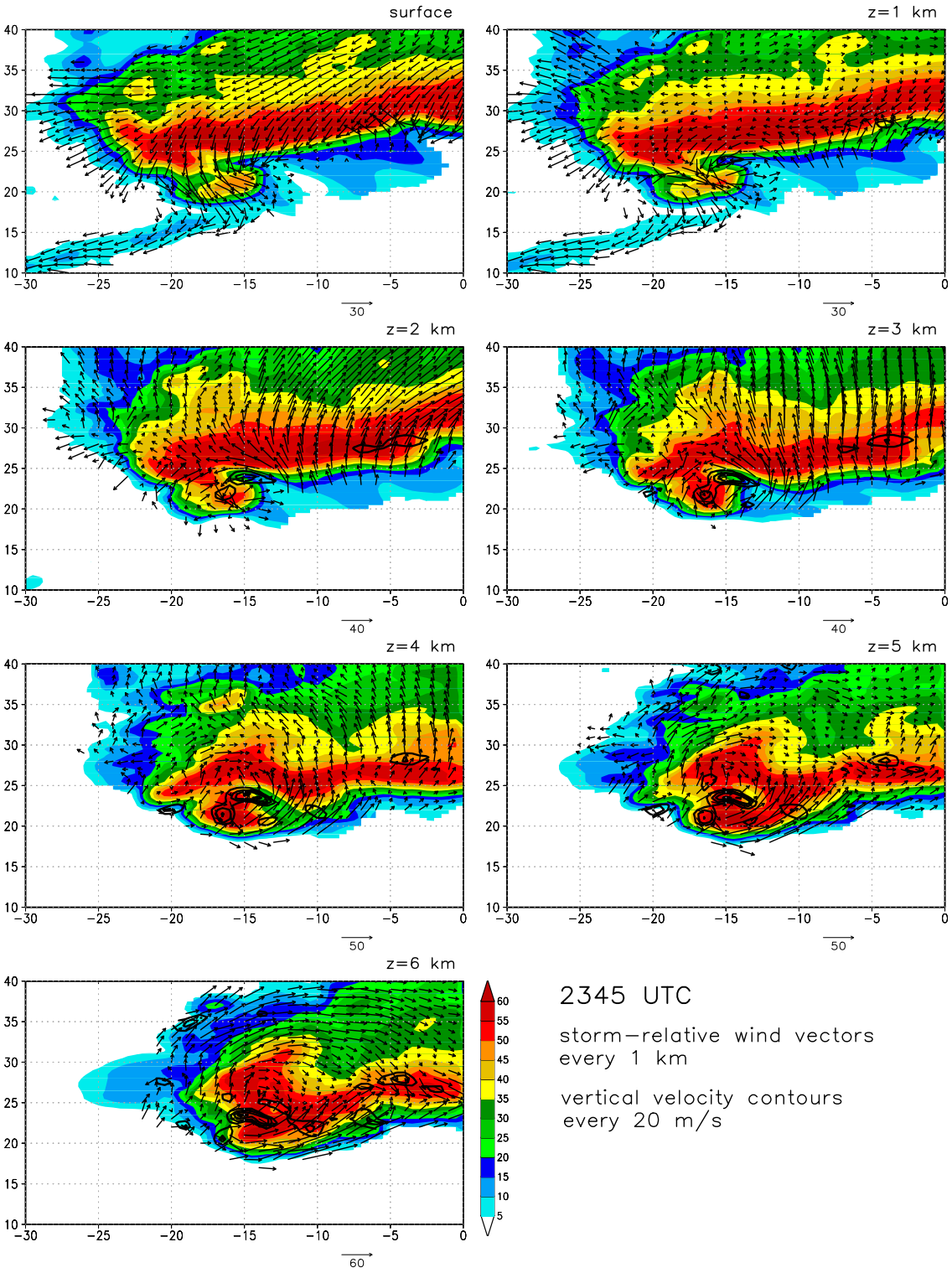

Figure 3: Horizontal cross-sections of radar reflectivity (shaded), storm-relative wind vectors, and vertical velocity (contoured every 20 ms^{-1}) from the surface through 6 km, every 1 km, at 2345 UTC. Note that the vector lengths vary with height. The x- and y-axes represent distance in km from the center of the grid.

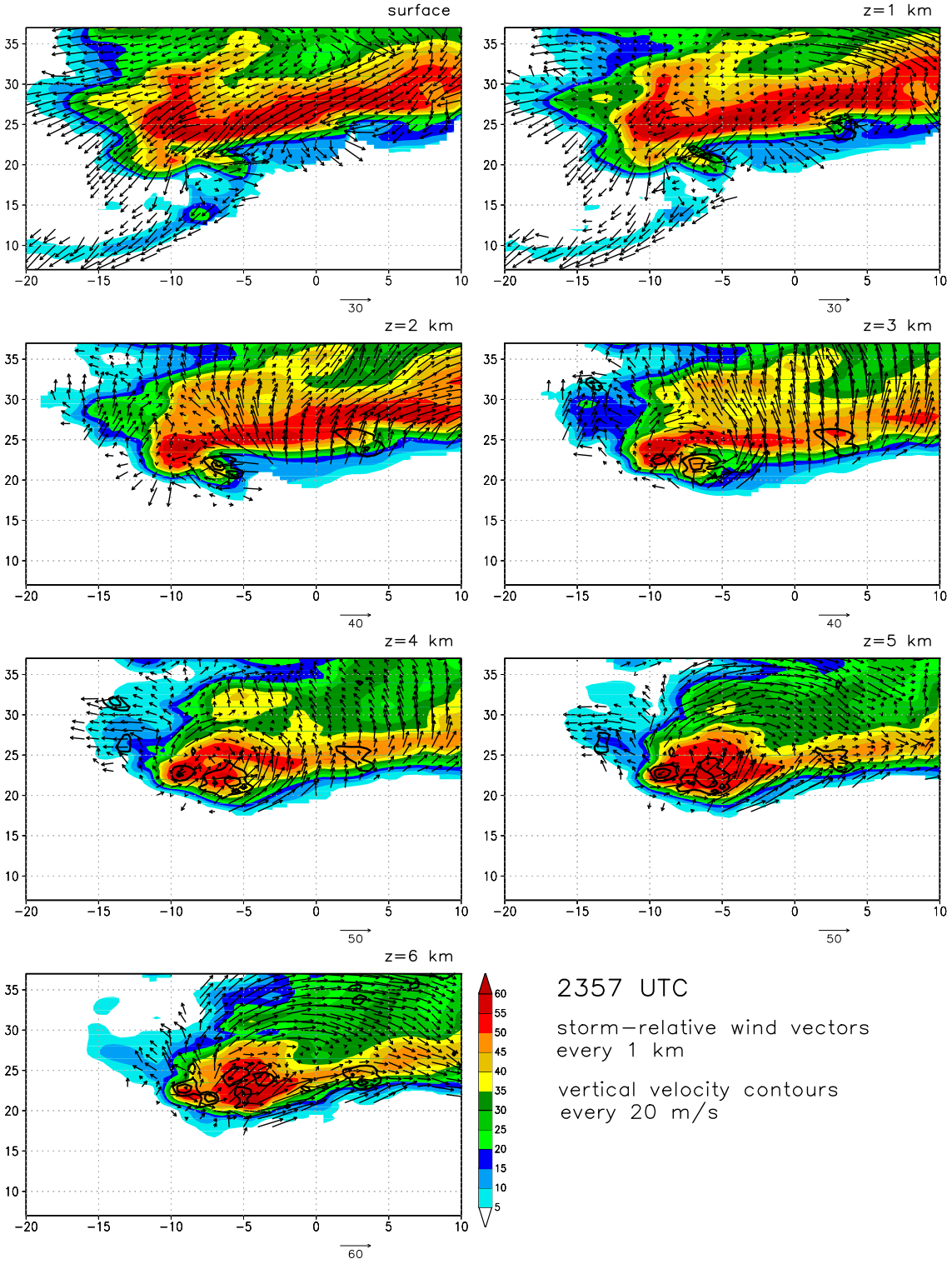

Figure 4: As in Fig. 3, but at 2357 UTC.

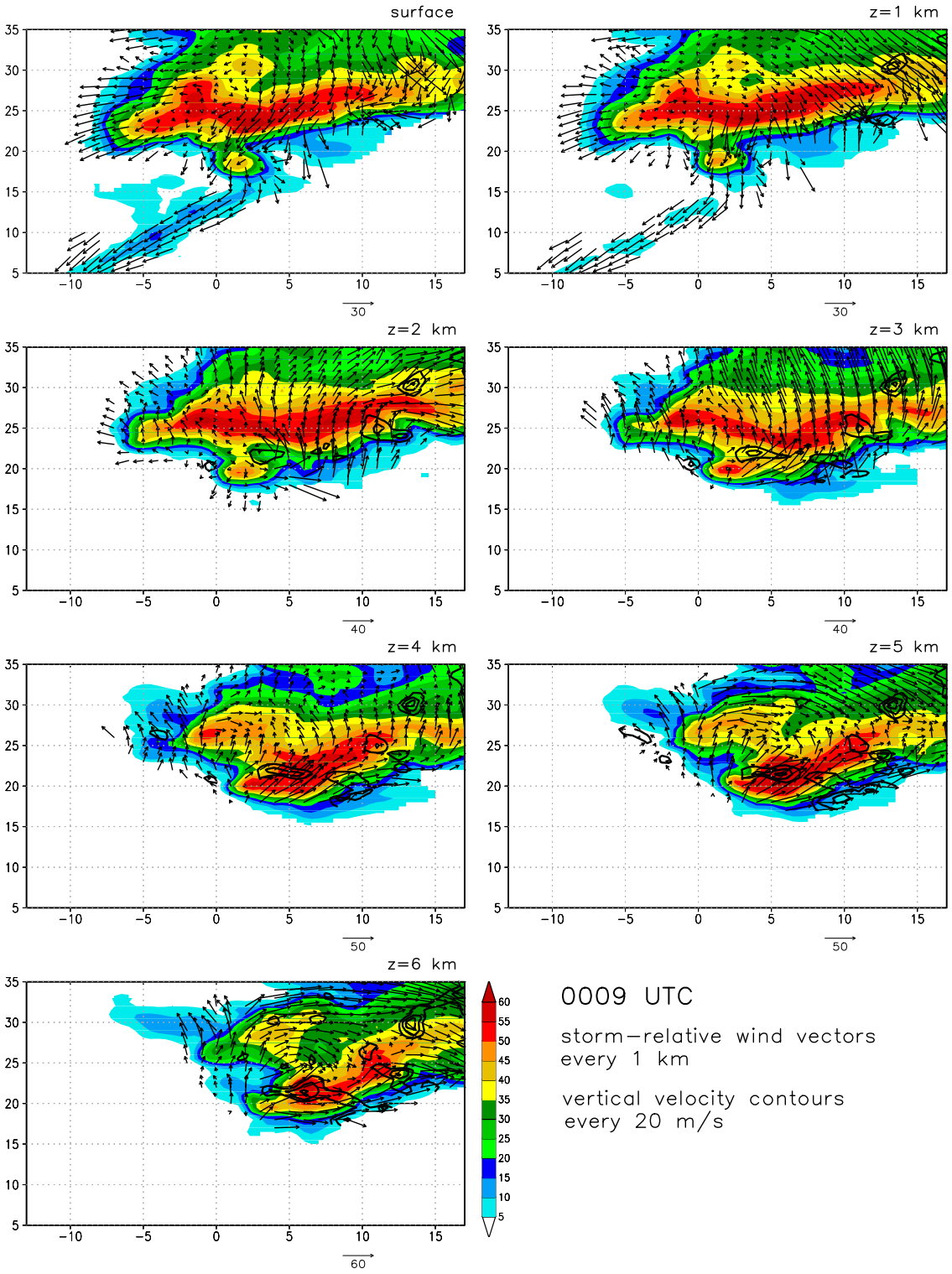

Figure 5: As in Fig. 3, but at 0009 UTC.

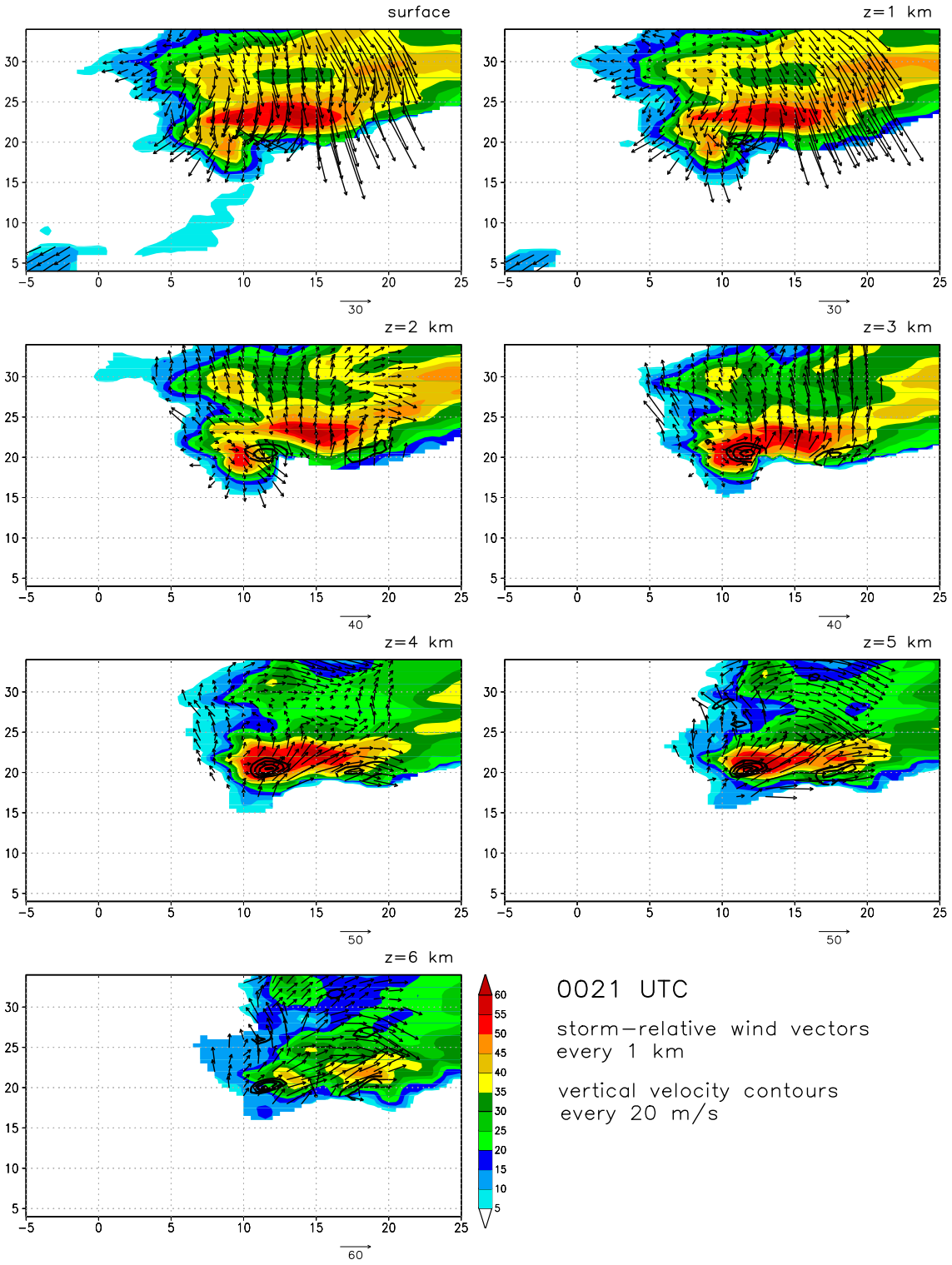

Figure 6: As in Fig. 3, but at 0021 UTC.

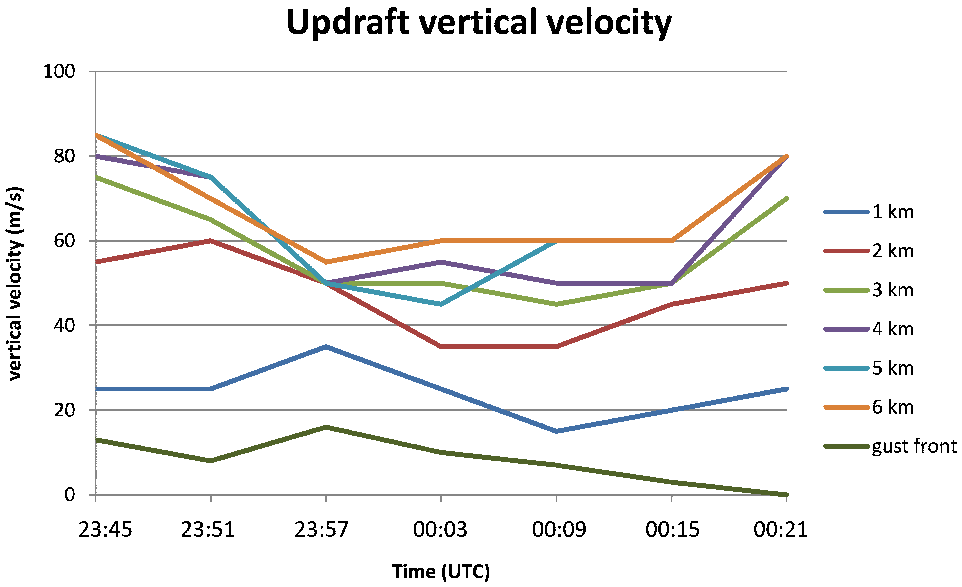

Figure 7: Time series of dual-Doppler derived updraft vertical velocities (ms^{-1}) at several heights. The maximum vertical velocity along the gust front is also plotted over time.

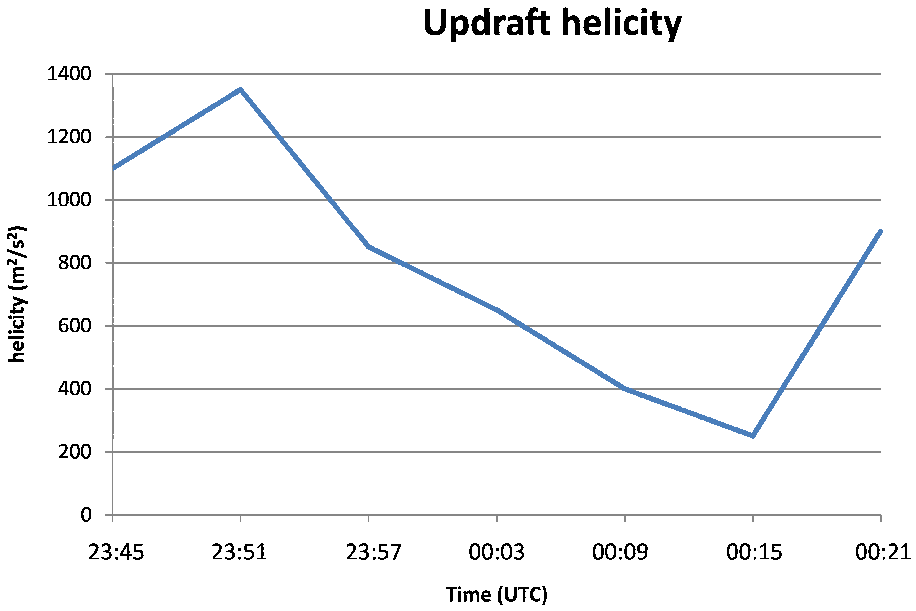

Figure 8: Time series of dual-Doppler derived updraft helicity (m^2s^{-2}), calculated in the manner of Kain et al. (2008).

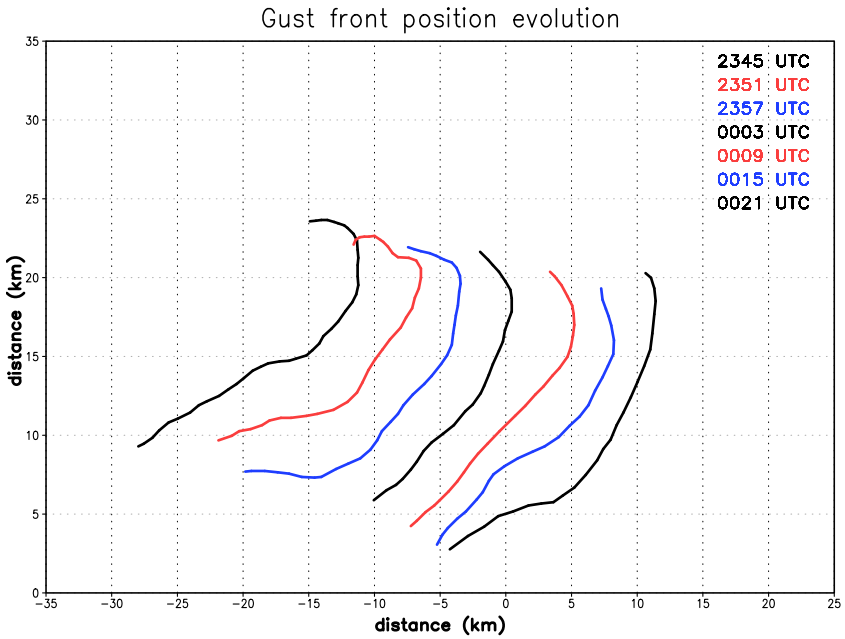

Figure 9: Evolution of the position of the rear flank gust front over time. The x- and y-axes represent the distance in km from the center of the grid (which is the position of SMART-R1).